Organic Electronics 10 (2009) 1442–1447

Contents lists available at ScienceDirect

Organic Electronics

journal homepage: www.elsevier.com/locate/orgel

The impact of self-assembled monolayer thickness in hybrid gate dielectrics for organic thin-film transistors

Abdesselam Jedaa [a], Martin Burkhardt [a], Ute Zschieschang [b], Hagen Klauk [b], Dana Habich [c], Günter Schmid [c], Marcus Halik [a,*]

[a] Department of Materials Science, University Erlangen – Nürnberg, Martensstr. 7, 91058 Erlangen, Germany
[b] Max Planck Institute for Solid State Research, Heisenbergstr. 1, 70569 Stuttgart, Germany
[c] Siemens AG CT MM 1, Günter-Scharowsky-Str. 1, 91058 Erlangen, Germany

ARTICLE INFO

Article history:
Received 6 June 2009
Received in revised form 7 August 2009
Accepted 7 August 2009
Available online 14 August 2009

PACS:
73.61

Keywords:
Self-assembled monolayer
Hybrid gate dielectrics
Organic thin film-transistor

ABSTRACT

We have investigated the electrical characteristics of hybrid dielectrics with a thickness of 6 nm or less that are composed of a plasma-grown aluminum oxide (AlO_x) layer and a self-assembled monolayer (SAM) of an aliphatic phosphonic acid. The impact of the quality of the AlO_x layer on the insulating properties of the double-layer dielectrics was assessed by comparing two different oxidation procedures, and the influence of the thickness of the organic SAM was evaluated by employing molecules with five different chain lengths. In order to decouple the relative contributions of the oxide and the SAM to the performance of the double-layer dielectrics we have also performed cyclic voltammetry measurements on indium tin oxide (ITO)/SAM devices without AlO_x layer. Finally, we have evaluated how the quality of the AlO_x layer and the thickness of the SAM affect the performance of low-voltage organic thin-film transistors (TFTs) that employ the thin AlO_x/SAM dielectrics as the gate dielectric. The results confirm the important role of the SAM in determining the breakdown voltage, in limiting the current density, and in compensating the somewhat lower quality of AlO_x layers produced under mild plasma conditions.

1. Introduction

Self-organizing molecules are promising components for the realization of a variety of functional layers in high-performance, low-cost, flexible electronic devices [1–7]. In the future, the process of molecular self-assembly may even outperform printing technologies in device fabrication, since the molecule-induced driving of voluntary film formation provides excellent positional and surface selectivity as well as full control over the film thickness. The properties of self-assembled monolayers (SAMs), in particular their chemical reactivity, packing density, and electrical performance, as well as the morphology of functional films deposited on top of the SAMs, depend critically on the choice of the self-organizing molecules [8–10]. For example, insulating SAMs in which the electrical current is controlled by the chain-length-dependent quantum-mechanical tunneling through an energy barrier have been realized using aliphatic alkanes grafted on metallically conducting electrodes (e.g. gold, hydrogen-terminated doped silicon, or doped gallium arsenide) [11–16]. Alternatively, alkane SAMs on silicon or aluminum terminated with a thin layer of native or plasma-grown oxide have been utilized as the gate dielectric in silicon field-effect transistors [17] and in organic thin-film transistors (TFTs) [2,18–24]. In these cases, the electrical current through the SAM is reduced compared to SAMs on gold or GaAs by the additional contribution of the thin oxide to the total insulator thickness. The current density through these low-temperature-processed thin oxide/

* Corresponding author. Tel.: +49 9131 8527732; fax: +49 9131 8528321.
E-mail address: marcus.halik@ww.uni-erlangen.de (M. Halik).

1566-1199/$ - see front matter © 2009 Elsevier B.V. All rights reserved.
doi:10.1016/j.orgel.2009.08.006

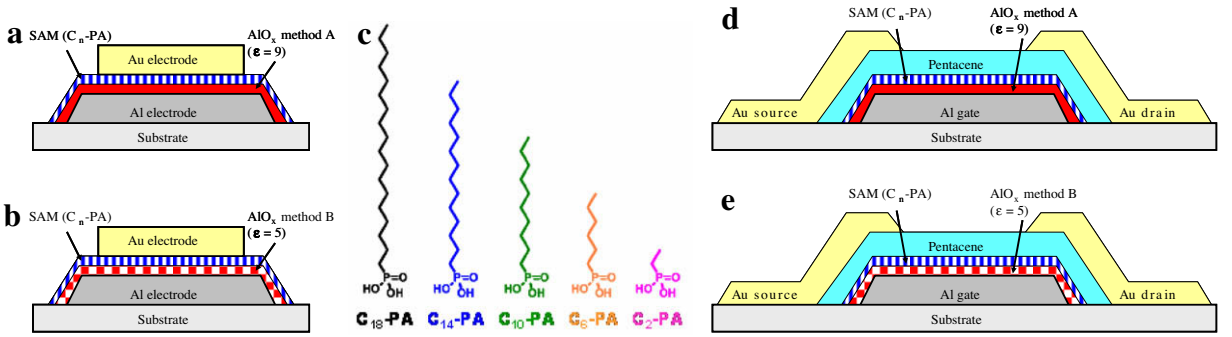

Fig. 1. Schematic cross sections of capacitors and thin-film transistors with thin AlO_x/SAM dielectric. (a) Capacitor with AlO_x grown by oxygen plasma (method A). (b) Capacitor with AlO_x grown by mild-air plasma (method B). (c) Chemical structures of *n*-alkyl phosphonic acids C_n-PA. (d) Pentacene TFT with AlO_x grown by oxygen plasma (method A). (e) Pentacene TFT with AlO_x grown by mild-air plasma (method B).

SAM dielectrics is comparable to or smaller than the current density through the gate dielectrics of modern silicon field-effect transistors that use high-temperature-grown inorganic gate oxides with a thickness of 2–3 nm [25,26].

In order to better understand the properties of the thin oxide/SAM double-layer dielectrics it is necessary to distinguish between the influence of the thin oxide and the influence of the molecular monolayer on the performance of the double-layer dielectric. In this work we compare the electrical characteristics of thin aluminum oxide/SAM double-layer dielectrics prepared using two different oxidation procedures and five different aliphatic phosphonic acids (Fig. 1c) on aluminum electrodes. To separate the effects of the oxide and the SAM on the insulating properties, we have performed current-voltage measurements on metal/oxide/SAM/metal capacitors and cyclic voltammetry measurements on ITO/SAM devices.

2. Experimental

The aluminum oxide (AlO_x) layers have a thickness of about 3.6 nm and the SAMs range in thickness from 0.4 to 2.4 nm. For each combination of oxidation procedure and SAM thickness, capacitor devices (Al/AlO_x/SAM/Au) and bottom-gate, top-contact pentacene organic TFTs (in which the AlO_x/SAM stack serves as the gate dielectric) were fabricated and characterized.

The aluminum electrodes were prepared by thermal evaporation of 30 nm thick aluminum through a stencil mask onto glass substrates. To create a thin AlO_x layer, the surface of the freshly evaporated aluminum was plasma-activated using one of two methods. Method A is an oxygen-plasma treatment performed in a turbo-pumped parallel-plate reactive ion etcher (process pressure: 0.1 mbar, plasma frequency: 13.56 MHz, plasma power: 200 W, duration: 30 s) that produces an AlO_x layer with a thickness of about 3.6 nm and a permittivity of nine [2]. Method B is a mild-air plasma (2 mbar, 40 kHz, 200 W, 120 s) which creates an AlO_x film with approximately the same thickness and surface roughness (rms roughness = 1.5 nm, measured by atomic force microscopy) as method A, but with smaller density and hence smaller permittivity (ε = 5). After the plasma treatment, the substrates were immersed in a 2-propanol solution containing 5 mM of one of five different alkyl phosphonic acids (dicyl-PA [C_2-PA], hexyl-PA [C_6-PA], decyl-PA [C_{10}-PA], tetradecyl-PA [C_{14}-PA], octadecxl-PA [C_{18}-PA]) to allow a monolayer with a thickness approximately proportional to the length of the molecule (assuming similar molecular tilt angles) to self-assemble on the hydroxyl-terminated surface of the plasma-oxidized aluminum. The solution was kept at room temperature, and substrates remained in solution for about 24 h. Substrates were then rinsed with 2-propanol, dried, and briefly baked at a temperature of 60 °C on a hotplate. Static contact angles of 105–110° were obtained for all films, except for the substrates with C_2-PA on which a slight corrosion of the aluminum patterns was observed and a smaller static contact angle of 80° was measured. The capacitors were completed by evaporating 30 nm thick gold through a stencil mask on top of the SAMs, resulting in capacitors with areas of $30 \times 30\ \mu m^2$, $50 \times 50\ \mu m^2$ and $100 \times 100\ \mu m^2$ (Fig. 1a and b). Organic TFTs were completed by evaporating 30 nm thick pentacene on top of the SAM-coated aluminum gate stack through a stencil mask, followed by evaporating 30 nm thick gold through another stencil mask to create the source/drain contacts (Fig. 1d and e). The pentacene TFTs have a channel length (L) of 30 μm and a channel width (W) of 450 μm.

For cyclic voltammetry measurements, the SAMs were prepared on ITO-coated glass substrates from solution with the same process described above for the Al/AlO_x/SAM/Au capacitors, but without an AlO_x layer and without a metal top contact. Static contact angles after SAM formation on ITO were similar to those for SAMs on aluminum oxide (105–115°). The ITO/SAM devices have an electrode area of 288 mm^2, which is much larger than the area of the Al/AlO_x/SAM/Au capacitors. The cyclic voltammetry measurements were carried out in a 0.9% NaCl(aq) solution using $K_3[Fe(CN)_6]$ as a redox-active indicator.

3. Results and discussion

3.1. Capacitor devices

To investigate the dielectric properties of the double-layer insulator stacks we have measured the capacitance

of each Al/AlO_x/SAM/Au device at frequencies from 10 kHz to 1 MHz and the current density through each stack as a function of applied voltage up to dielectric breakdown. Each measurement was repeated on at least four capacitors. The results are independent of the capacitor cell area. The measured capacitances are summarized in Table 1 and compared with the capacitances calculated using the equation $C_{total} = 1/(1/C_{SAM} + 1/C_{AlO_x})$ assuming a permittivity of 2.5 for the SAM [27], a permittivity of nine for the oxygen-plasma-grown AlO_x, a permittivity of five for the mild-air-plasma-grown AlO_x, a thickness of 3.6 nm for the AlO_x, and a thickness between 0.41 and 2.44 nm for the SAM, depending on alkyl chain length. The measured capacitances are between 0.38 μF/cm^2 for mild-air-plasma-grown AlO_x/C_{18}-PA SAM and 1.75 μF/cm^2 for oxygen-plasma-grown AlO_x/C_2-PA SAM, and they are in good agreement with the calculated values.

Fig. 2 shows the measured current density as a function of applied voltage. For the series of capacitors with oxygen-plasma-grown AlO_x ($\varepsilon = 9$; see Fig. 2a), the breakdown voltage is essentially the same (4.4 V) for devices without SAM and devices with short SAM (C_6-PA, C_2-PA). When the SAM chain length is increased to C_{10} and beyond, a monotonic increase in breakdown voltage is observed, up to 5 V for C_{18}-PA. With the exception of the devices with C_2-PA (which appears to corrode the aluminum) the current density at low voltages (~1–2 V) is similar for all devices with SAM regardless of chain length and slightly smaller than for devices without SAM (4×10^{-7} A/cm^2 at 1 V; 4×10^{-6} A/cm^2 at 2 V). When the voltage is increased beyond 2 V, the increase in current density with increasing voltage is greater for the devices with shorter SAM chain length than for those with longer SAM chain length. At large voltage (~4 V), the current density through the devices with C_{18}-PA SAM is two orders of magnitude smaller than through the devices without SAM, confirming the important role of the SAM in limiting the current density.

The devices based on mild-air-plasma-grown AlO_x ($\varepsilon = 5$) show slightly different results (see Fig. 2b). Most significantly, the devices without SAM have a smaller breakdown voltage and a larger current density than the oxygen-plasma-grown AlO_x without SAM (breakdown voltage is 4 V instead of 4.4 V; current density at 2 V is 1×10^{-1} A/cm^2 instead of 2×10^{-5} A/cm^2). We attribute these findings to the lower quality of the mild-air-plasma-grown AlO_x compared with the oxygen-plasma-grown AlO_x (lower density, larger number of leakage paths). Consequently, the devices with mild-air-plasma-grown AlO_x and SAM also show larger current density than the oxygen-plasma-grown AlO_x/SAM devices. In the devices with C_{10}-PA, C_{14}-PA and C_{18}-PA SAM the current density at 2 V is larger by about one order of magnitude (~3×10^{-5} A/cm^2 instead of 4×10^{-6} A/cm^2), while the devices with C_6-PA SAM show a more pronounced dependence on the oxide quality and hence a current density that is more than two orders of magnitude larger (8×10^{-4} A/cm^2 instead of 4×10^{-6} A/cm^2 at 2 V) than for the devices with oxygen-plasma-grown AlO_x. This indicates that at least for the longer alkyl chains the lower quality of the mild-air-plasma-grown AlO_x is compensated by the SAMs. When the voltage is increased beyond 2 V, the increase in current density with increasing voltage is essentially the same for the devices with C_{10}-PA, C_{14}-PA and C_{18}-PA SAM, while the breakdown voltage shows the same trend with SAM chain length as in the series with oxygen-plasma-grown AlO_x, indicating that the electrical properties at large electrical fields are dominated by the SAMs, rather than the oxide. Due to the smaller permittivity of the mild-air-plasma-grown AlO_x, the capacitance measured in these devices is smaller, but follows the trend related to the contribution of the SAM chain length (see Table 1).

3.2. Cyclic voltammetry

To study the chain-length-dependent insulating properties of the phosphonic acid SAMs without the contribution of the insulating metal oxide (AlO_x) we have also prepared monolayers of C_6-PA, C_{10}-PA and C_{18}-PA SAMs on conducting indium tin oxide (ITO) electrodes and performed cyclic voltammetry (CV) measurements. Note that in contrast to the Al/AlO_x/SAM/Au capacitors discussed in the previous section, the ITO/SAM devices for the cyclic voltammetry analysis have no AlO_x layer and no Au contact. Therefore, any pinholes present in the SAM would be permeable for the electrolyte and thus result in a substantial leakage current that would be expected to be independent of the alkyl chain length. On the other hand, if the pinhole density is negligible, the currents through the SAM will be due to

Table 1
Electrical parameters of capacitors and pentacene TFTs.

		C_{18}-PA (2.44 nm)[a]	C_{14}-PA (1.95 nm) [a]	C_{10}-PA (1.43 nm) [a]	C_6-PA (0.91 nm) [a]	C_2-PA (0.41 nm) [a]
Capacitance (meas.)(μF/cm^2)	Oxidation	0.67	0.8	0.86	1	1.75
Capacitance (calc.)(μF/cm^2)	**Method A**	0.64	0.75	0.91	1.15	1.56
Mobility (cm^2/Vs)	(Oxygen plasma)	0.18	0.28	0.15	0.05	–
I_D/I_G	AlO_x	5×10^3	7×10^3	2×10^3	2×10^2	–
On/off ratio	($\varepsilon = 9$)	7×10^5	2×10^6	2×10^6	2×10^4	–
Capacitance (meas.)(μF/cm^2)	Oxidation	0.38	0.6	0.78	0.86	0.9
Capacitance (calc.)(μF/cm^2)	**Method B**	0.52	0.59	0.68	0.81	1
Mobility (cm^2/Vs)	(Mild-air plasma)	0.17	0.13	0.03	–	–
I_D/I_G	AlO_x	2×10^2	9×10^1	7	–	–
On/off ratio	($\varepsilon = 5$)	2×10^6	3×10^5	5×10^3	–	–

[a] Calculated using CambridgeSoft Chem3D Pro; www.cambridgesoft.com.

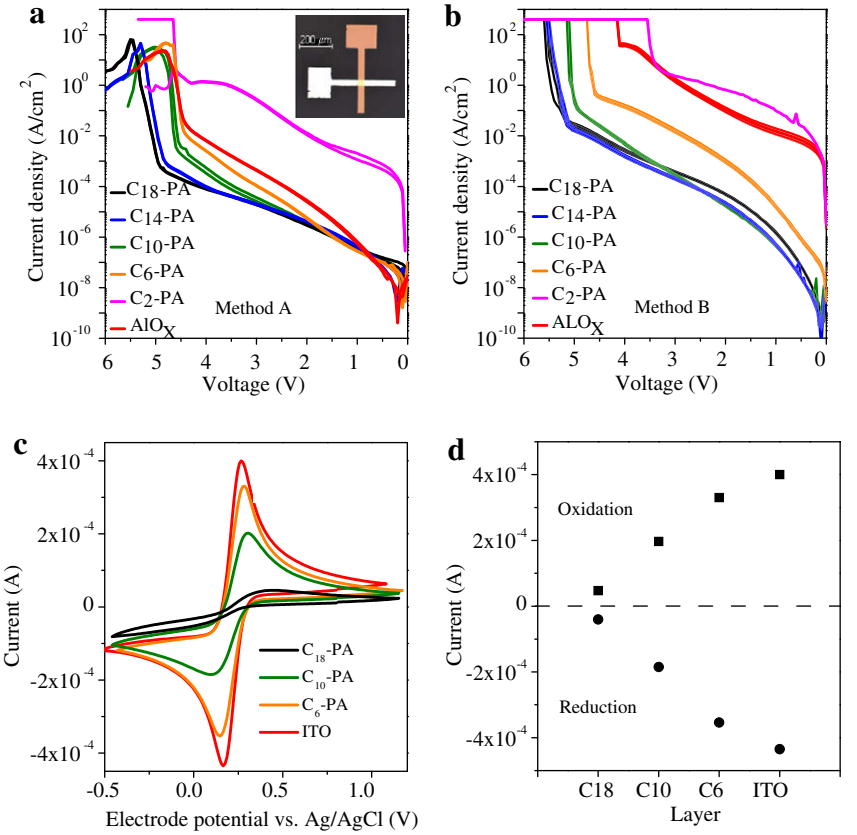

Fig. 2. Current density as a function of voltage of Al/AlO_x/SAM/Au capacitors with an area of 50 × 50 μm. (a) AlO_x grown by oxygen plasma (method A). Inset: photographic image of a capacitor. (b) Capacitor with AlO_x grown by mild-air plasma (method B). (c) CV of SAM-coated ITO electrodes in 0.9% NaCl (aq.) with $K_3[Fe(CN)_6]$ redox indicator (50 mV/s, Ag/AgCl and Pt counter electrode). (d) CV-current of the oxidation and reduction peaks vs. alkyl chain length of the SAM.

quantum-mechanical tunneling, with a monotonic dependence on the molecular chain length.

The experimental results are summarized in Fig. 2c and d. In all measurements, the redox behavior is reversible, without noticeable damage to the organic monolayers. The results show that the indicator response decreases monotonically with increasing molecular chain length. The CV measurements thus confirm the conclusions from the Al/AlO_x/SAM/Au capacitor measurements, namely that the insulating properties of the SAMs are indeed a strong, monotonic function of the molecular chain length.

3.3. Organic transistors

In a field-effect transistor, the voltage-dependent current through the gate dielectric leads to an undesired gate current during device operation. Thus, for transistors the quality of the dielectric is best described by the gate current (I_G) and by the ratio between the drain current and the gate current (I_D/I_G) as a function of gate-source voltage (V_{GS}).

The gate currents as a function of gate-source voltage of pentacene TFTs based on oxygen-plasma-grown AlO_x ($\varepsilon = 9$) with four different SAMs (C_6-PA, C_{10}-PA, C_{14}-PA and C_{18}-PA) are shown in Fig. 3a. The drain currents as a function of gate-source voltage of the same TFTs are shown in Fig. 3b. In general, these devices exhibit small gate currents and large I_D/I_G ratios, as observed previously for C_{18}-PA SAMs on oxygen-plasma-grown AlO_x [2]. However, a monotonic increase in gate current is observed as the SAM chain length is reduced from C_{18}-PA to C_{14}-PA, C_{10}-PA and C_6-PA (1.5×10^{-10} A, 3.7×10^{-10} A, 6.1×10^{-10} A and 3.2×10^{-9} A at $V_{GS} = -2.5$ V). In devices with C_2-PA SAM the gate current exceeds the drain current, making these devices unsuitable for practical applications. For each TFT the charge carrier mobility was calculated in the saturation regime using the standard formalism for field-effect transistors: $\mu = 2\,L/(W \cdot C_{diel}) \cdot (\delta I_D/\delta V_{GS})^2$, where C_{diel} is the measured dielectric capacitance, I_D is the drain current, and V_{GS} is the gate-source voltage. Mobilities of 0.18 cm^2/Vs for C_{18}-PA, 0.28 cm^2/Vs for C_{14}-PA and 0.15 cm^2/Vs for C_{10}-PA were calculated for the TFTs with oxygen-plasma-grown AlO_x. Devices based on C_6-PA exhibit a notably smaller mobility of 0.05 cm^2/Vs. In addition to the mobility and the ratio between drain current and gate current (I_D/I_G), Table 1 also lists the ratio between the maximum and the minimum drain current (on/off ratio) of each TFT.

The TFTs with mild-air-plasma-grown AlO_x/SAM gate dielectrics (permittivity of $AlO_x = 5$) show a larger gate leakage compared to the TFTs with oxygen-plasma-grown

AlO_x (see Fig. 4). To prevent the gate currents from exceeding 10 nA these TFTs were measured only up to a maximum gate-source voltage of −2 V. In addition to the generally larger gate currents, the increase in gate current with reduced SAM chain length from C_{18}-PA to C_{14}-PA and C_{10}-PA is more pronounced (7.3×10^{-10} A, 3.4×10^{-9} A and 1.5×10^{-8} A at $V_{GS} = -2.0$ V). As a consequence, the I_D/I_G ratio is smaller by about one to two orders of magnitude than in TFTs with oxygen-plasma-grown AlO_x (see Table 1). As a result of this trend, the C_{14}-PA SAM is a lower limit in terms of the minimum chain length for the mild-plasma-grown oxide. In TFTs with C_2-PA SAM (aluminum corrosion) and C_6-PA SAM the gate current exceeds the drain current, in line with the trend observed for the current density in the capacitors. Using the measured capacitance values, charge carrier mobilities of 0.17 cm^2/Vs for C_{18}-PA, 0.13 cm^2/Vs for C_{14}-PA and 0.03 cm^2/Vs for C_{10}-PA have been calculated.

For both series of TFTs (oxygen-plasma-grown AlO_x, mild-air-plasma-grown AlO_x) the mobility decreases as the alkyl chain length of the SAM is reduced from C_{14}-PA to C_{10}-PA and to C_6-PA. This indicates that the ordering in the SAM is systematically reduced as the alkyl chain length and hence the strength of the cohesive interactions between the phosphonic acid molecules is reduced [28], since less ordering in the SAM is likely to also induce less ordering in the pentacene layer and thus lower mobility.

Hill et al. have recently reported pentacene TFTs with a 100 nm thick SiO_2 gate dielectric obtained by thermal oxidation of the silicon substrate and functionalized with alkyl phosphonic acid SAMs with alkyl chain length ranging from C_6-PA to C_{18}-PA [29]. Due to the excellent insulation provided by the thick SiO_2 layer, the gate current in these TFTs is insignificant. The largest mobility was obtained with a C_8-PA SAM (1.2 cm^2/Vs). As the chain length was increased from C_8-PA to C_{18}-PA, the mobility decreased monotonically to 0.2 cm^2/Vs. For TFTs with a C_6-PA SAM a mobility of 0.5 cm^2/Vs was reported. It appears that the trend of the mobility as a function of alkyl chain length observed by Hill et al. is quite different from the one we have observed in our TFTs. However, the results are not easily compared, since the mechanisms that con-

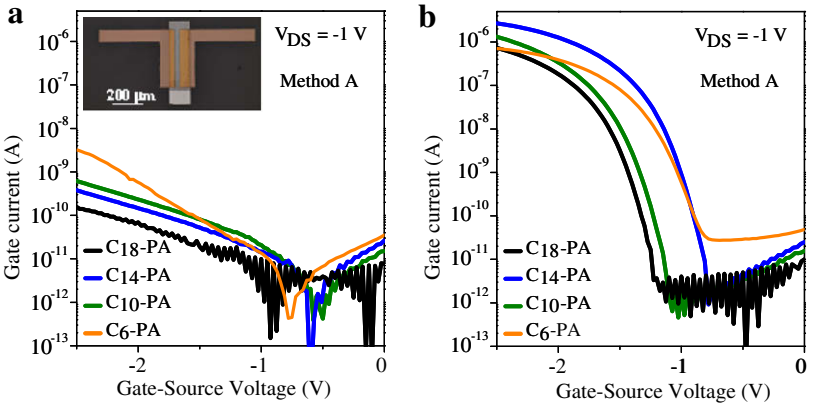

Fig. 3. Electrical characteristics of pentacene TFTs with oxygen-plasma-grown AlO_x/SAM gate dielectrics (method A). (a) Gate current as a function of gate-source voltage. Inset: Photograph of a TFT. (b) Drain current as a function of gate-source voltage.

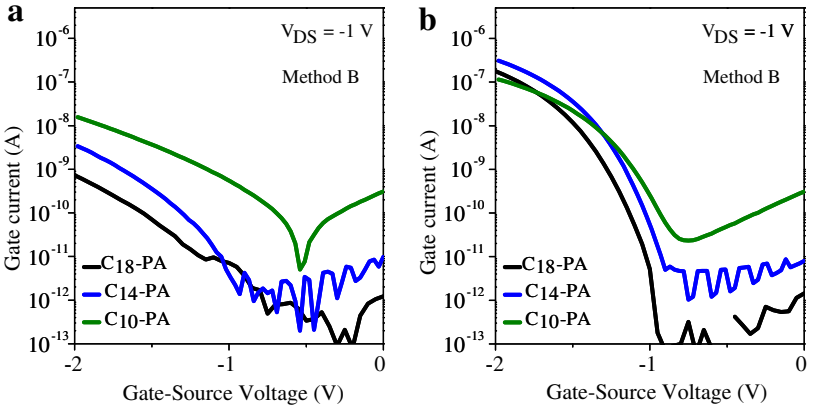

Fig. 4. Electrical characteristics of pentacene TFTs with mild-air-plasma-grown AlO_x/SAM gate dielectrics (method B). (a) Gate current as a function of gate-source voltage. (b) Drain current as a function of gate-source voltage.

trol adsorption, binding, and monolayer formation of alkyl phosphonic acids on aluminum oxide and on silicon dioxide are fundamentally different [30], and so the microscopic structure of the monolayers is expected to be quite different as well.

4. Conclusion

We have demonstrated that varying the molecular chain length (n) of aliphatic C_n-phosphonic acids influences the electrical characteristics of SAMs based on these molecules. In capacitors that utilize AlO_x/SAM stacks as double-layer dielectrics the breakdown voltage correlates with the chain length of the self-assembling molecules, while the current density at low fields and the increase in current density with increasing voltage are determined by the quality of the thin AlO_x layer underneath the SAM. The important role of the chain length of the organic self-assembling molecules in determining the insulating properties of the monolayers has been confirmed using cyclic voltammetry measurements on large-area ITO/SAM devices. Similar trends were found for the gate current in pentacene TFTs that utilize an AlO_x/SAM stack as the gate dielectric. Reliable low-voltage transistor operation with mobility greater than 0.1 cm^2/Vs has been observed for gate dielectrics with C_{18}-PA and C_{14}-PA SAM on AlO_x of different quality. When using a high-quality oxygen-plasma-grown AlO_x, the SAM approach can be extended to SAMs as short as C_{10}-PA. This suggests that low-cost processes for the activation of the metal gate electrodes are suitable and that alkyl chains shorter than C_{18} provide adequate insulating properties for large-area devices.

Acknowledgements

We thank T. Erlbacher for expert technical assistance. Partial financial support (A.J. and M.B.) was provided by the Deutsche Forschungsgemeinschaft (grant DFG-HA 2952/2). Additional we thank to the Cluster of Excellence "Engineering of Advanced Materials".

References

[1] H.B. Akkerman, P.W.M. Blom, D.M. De Leeuw, B. De Boer, Nature 441 (2006) 69–71.
[2] H. Klauk, U. Zschieschang, J. Pflaum, M. Halik, Nature 445 (2007) 745–748.
[3] M. Mottaghi, P. Lang, F. Rodriguez, A. Rumyantseva, A. Yassar, G. Horowitz, S. Lenfant, D. Tondelier, D. Vuillaume, Adv. Funct. Mater. 17 (2007) 597–604.
[4] D.J. Gundlach, L. Jia, T.N. Jackson, IEEE Electr, IEEE Electr. Dev. Lett. 22 (2001) 571–573.
[5] S. Kobayashi, T. Nishikawa, T. Takenobu, S. Mori, T. Shimoda, T. Mitani, H. Shimotani, N. Yoshimoto, S. Ogawa, Y. Iwasa, Nat. Mater. 3 (2004) 317–322.
[6] A.L. Briseno, S.C.B. Mannsfeld, M.M. Ling, S. Liu, R.J. Tseng, C. Reese, M.E. Roberts, Y. Yang, F. Wudl, Z. Bao, Nature 444 (2006) 913–917.
[7] U. Zschieschang, M. Halik, H. Klauk, Langmuir 24 (2008) 1665–1669.
[8] A. Ulman, An Introduction to Ultrathin Films: From Langmuir–Blodgett to Self-Assembly, Academic Press, Boston, 1991 (Part 3).
[9] M.H. Yoon, A. Facchetti, T.J. Marks, Proc. Natl. Acad. Sci. USA 102 (2005) 4678.
[10] K.P. Pernstich, S. Haas, D. Oberhoff, C. Goldmann, D.J. Gundlach, B. Batlogg, A.N. Rashid, G. Schitter, J. Appl. Phys. 96 (2004) 6431–6437.
[11] H.B. Akkerman, R.C.G. Naber, B. Jongbloed, P.A. van Hal, P.W.M. Blom, D.M. De Leeuw, B. De Boer, Proc. Natl. Acad. Sci. USA 104 (2007) 11161–11166.
[12] J.M. Buriak, Chem. Rev. 102 (2002) 1271–1308.
[13] Y.-L. Loo, J.W.P. Hsu, R.L. Willett, K.W. Baldwin, K.W. West, J.A. Rogers, et al., J. Vac. Sci. Technol. B 20 (2002) 2853–2856.
[14] H.B. Akkerman, A.J. Kronemeijer, P.A. van Hal, P.W.M. Blom, D.M. De Leeuw, B. De Boer, Small 4 (2008) 100–104.
[15] P.A. van Hal, E.C.P. Smits, T.C.T. Geuns, H.B. Akkerman, B.C. De Brito, S. Perissinotto, G. Lanzani, A.J. Kronemeijer, V. Geskin, J. Cornil, P.W.M. Blom, B. De Boer, D.M. De Leeuw, Nat. Nanotechnol. 3 (2008) 749–754.
[16] G. Robert, V. Derycke, M.F. Goffman, S. Lenfant, D. Vuillaume, J.-P. Bourgoin, Appl. Phys. Lett. 93 (2008) 143117.
[17] J. Collet, D. Vuillaume, Appl. Phys. Lett. 73 (1998) 2681–2683.
[18] J. Collet, O. Tharaud, A. Chapoton, D. Vuillaume, Appl. Phys. Lett. 76 (2000) 1941–1943.
[19] M. Halik, H. Klauk, U. Zschieschang, G. Schmid, C. Dehm, M. Schutz, S. Malsch, F. Effenberger, M. Brunnbauer, F. Stellacci, Nature 431 (2004) 963–966.
[20] Y.D. Park, D.H. Kim, Y. Jang, M. Hwang, J.A. Lim, K. Cho, Appl. Phys. Lett. 87 (2005) 243509.
[21] D.H. Kim, J.T. Han, Y.D. Park, Y. Jang, J.H. Cho, M. Hwang, K. Cho, Adv. Mater. 18 (2006) 719–723.
[22] K.D. Kim, C.K. Song, Appl. Phys. Lett. 88 (2006) 233508.
[23] H. Ma, O. Acton, G. Ting, J.W. Ka, H.-L. Yip, N. Tucker, R. Schofield, A.K.-Y. Jen, Appl. Phys. Lett. 92 (2008) 113303.
[24] P.H. Wöbkenberg, J. Ball, F.B. Kooistra, J.C. Hummelen, D.M. De Leeuw, D.D.C. Bradley, T.D. Anthopoulos, Appl. Phys. Lett. 93 (2008) 013303.
[25] K. Sekine, Y. Saito, M. Hirayama, T. Ohmi, IEEE Trans. Electr. Dev. 48 (2001) 1550–1555.
[26] S.-H. Lo, D.A. Buchanan, Y. Taur, W. Wang, IEEE Eletr. Dev. Lett. 18 (1997) 209–211.
[27] P. Fontaine, D. Goguenheim, D. Deresmes, D. Vuillaume, M. Garet, F. Rondelez, Appl. Phys. Lett. 62 (1993) 2256–2258.
[28] D.M. Spori, N.V. Venkataraman, S.G.P. Tosatti, F. Durmaz, N.D. Spencer, S. Zürcher, Langmuir 23 (2007) 8053–8060.
[29] I.G. Hill, C.M. Weinert, L. Kreplak, B.P. van Zyl, Appl. Phys. A 95 (2009) 81–87.
[30] E.L. Hanson, J. Schwartz, B. Nickel, N. Koch, M.F. Danisman, J. Am. Chem. Soc. 125 (2003) 16074–16080.